Article:
Julrat, S, Chongcheawchamnan, M, Khaoraphapong, T et al. (1 more author) (2012) Analysis and design of a differential sampled-line six-port reflectometer. IEEE Transactions on Microwave Theory and Techniques, 61 (1). 244 - 255. ISSN 0018-9480

https://doi.org/10.1109/TMTT.2012.2227788

Analysis and Design of a Differential Sampled-Line Six-Port Reflectometer

Sakol Julrat, Mitchai Chongcheawchamnan *Senior Member*, *IEEE*, Thanate Khaoraphapong, and Ian D. Robertson *Fellow*, *IEEE*

Abstract—**The analysis and design of a differential six-port reflectometer (SPR) based on a sampled-line structure is presented in this paper. The practical differential SPR is realized in Coplanar Strip (CPS) transmission line form, using two baluns for interfacing with the RF source and device under test (DUT) and four baluns connected to the RF logarithmic detectors. The performance of the proposed differential SPR structure is evaluated with a common-mode rejection ratio analysis and impedance measurement. A prototype differential SPR was designed and fabricated at 1 GHz in order to verify the analysis. Measurement results for various load impedances are compared with the measured results obtained from a commercial automatic vector network analyzer. It is shown that the differential structure gives a significant advantage in rejecting common-mode interference signals.**

Index Terms—Reflectometry, microwave measurements, impedance measurement, transmission line measurements

I. Introduction

The six-port reflectometer (SPR) is well known in the field of microwave measurements and sensing. The technique determines the complex reflection coefficient of a device under test (DUT) from four signal amplitude measurements. Since phase does not need to be measured directly, RF detectors can be used and a low cost measurement [1]-[3] system can be realized. There are several low-cost applications that can use SPR, such as dielectric permittivity measurement [4]-[5], moisture content determination [6]-[8], breast cancer detection [9], imaging sensors [10] and radar systems [11]-[13], to name but a few.

Previously, most SPRs have been implemented as single-ended designs which are fundamentally sensitive to electromagnetic interference, ground bouncing, substrate noise, etc. This will be manifested as common-mode noise in a differential system. It is well known that the common-mode rejection can be considerably improved by using a differential measurement technique [14]. From a circuit implementation viewpoint, a differential circuit outperforms the single-ended circuit in terms of a capability to reduce common-mode noise and offers higher dynamic range [15]. Thus, to effectively reduce these unwanted signals and enhance dynamic range in an SPR system, a differential technique should be applied to the design. The key to achieve this is to use a differential structure and develop a reflection coefficient determination algorithm based on the differential-mode network.

In this paper, mixed-mode S-parameter analysis is used to study the concept of the differential SPR structure and establish a method to determine the reflection coefficient. The SPR performance is considered in terms of common-mode rejection ratio (CMRR). The structure proposed in [16] is used to demonstrate the feasibility of the concept since it can readily be applied to a differential SPR structure with sufficient accuracy for many applications. In Section II, the differential SPR structure is analyzed with mixed-mode S-parameters and the methods for determining reflection coefficient and calibration are presented. An analysis of common-mode rejection ratio for the differential SPR structure is presented and discussed in Section III. The design and simulation results of the differential SPR structure are given in Section IV. The differential SPR structure is designed and fabricated to operate at 1 GHz on FR4 substrate. Experimental results of this prototype are used to validate the concept in Section V. Finally, the paper will be concluded in Section VI.

II. Differential SPR Concept

The proposed SPR system based on a differential structure is illustrated in Fig. 1. The differential SPR structure is composed of a six-port network operating in differential mode; ports 1 and 2 of the differential six-port network are connected to baluns that connect to the RF source and DUT, respectively. Four more baluns are employed, one for each signal power measurement port, numbers 3 to 6. The outputs from these four baluns are connected to RF detectors and the DC outputs are used to determine the reflection coefficient.

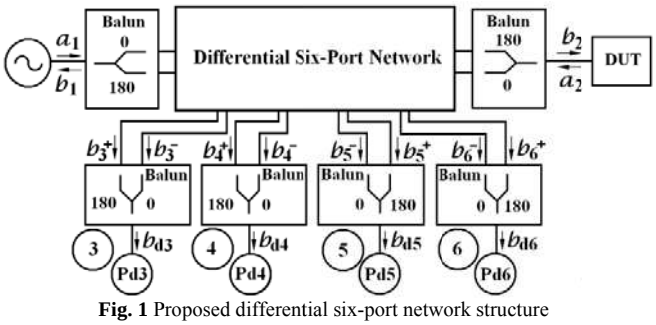

Fig. 1 Proposed differential six-port network structure

Manuscript received xxxxxxx

S. Julrat, M. Chongcheawchamnan and T. Khaorapapong are with the Department of Computer Engineering, Faculty of Engineering, Prince of Songkla University, Songkhla, 90112, Thailand. (corresponding author e-mail: mitchai@coe.psu.ac.th).

I. D. Robertson is with the Institute of Microwaves and Photonics, University of Leeds, Leeds LS2 9JT, UK

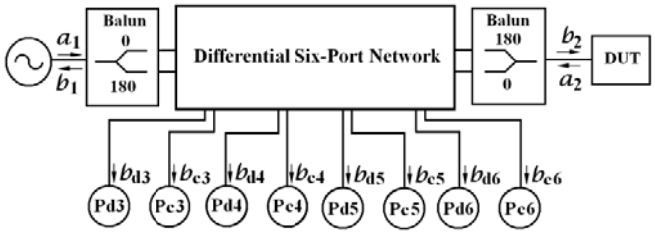

Fig. 2 Conceptual schematic of the differential SPR

A. Mixed-mode S-parameter analysis

To analyze the proposed differential SPR shown in Fig. 1, mixed-mode S-parameters are adopted to describe the differential and common-mode signals. Fig. 2 illustrates the schematic diagram defining the various wave parameters for the differential SPR. From Fig. 2, a_n and b_n represent the reflected and incident waves, respectively, at single-ended port n [17]. a_{dn} and b_{dn} are the differential-mode incident and reflected waves at differential port n. a_{cn} and b_{cn} are the common-mode incident and reflected waves at common-mode port n [14]. The conversion between single-ended and differential wave variable can be found in [18]. P_{dn} and P_{cn} are differential and common mode power wave at differential port n, respectively.

To obtain the power wave equation of the proposed differential SPR structure in Fig. 2, the wave variable equations can be defined as follows,

$$b_1 = S_{11}a_1 + S_{12}a_2 \quad (1a),$$
$$b_2 = S_{21}a_1 + S_{22}a_2 \quad (1b),$$
$$b_{dk} = S_{dk1}a_1 + S_{dk2}a_2 \quad (1c),$$
$$b_{ck} = S_{ck1}a_1 + S_{ck2}a_2 \quad (1d),$$

where k = 3,4,5 and 6 denotes the detector port number. S_{11}, S_{12}, S_{21}, and S_{22} are single-ended S-parameters of the differential SPR. S_{dk1} and S_{dk2} are mixed-mode S-parameters representing the transmission coefficients from the single-ended port 1 and 2 to the differential port k, respectively. S_{ck1} and S_{ck2} are mixed-mode S-parameters representing the transmission coefficients from the single-ended signal port 1 and 2 to the common-mode port k, respectively.

Rewriting (1b) in terms of a_1 and applying this to (1c) and (1d), we obtain,

$$b_{dk} = \left(S_{dk2} - \frac{S_{dk1}S_{22}}{S_{21}}\right)a_2 + \left(\frac{S_{dk1}}{S_{21}}\right)b_2 \quad (2a),$$

$$b_{ck} = \left(S_{ck2} - \frac{S_{ck1}S_{22}}{S_{21}}\right)a_2 + \left(\frac{S_{ck1}}{S_{21}}\right)b_2 \quad (2b).$$

Since the reflection coefficient of the DUT (Γ) is equal to a_2/b_2, (2a) and (2b) can be rewritten in the power wave equation form as follows,

$$|b_{dk}|^2 = |A_{dk}\Gamma + B_{dk}|^2|b_2|^2 \quad (3a),$$
$$|b_{ck}|^2 = |A_{ck}\Gamma + B_{ck}|^2|b_2|^2 \quad (3b),$$

where $|b_{dk}|^2$ and $|b_{ck}|^2$ are differential and common-mode power waves at port k, respectively. A_{dk} and B_{dk} are the characteristic parameters of the differential six-port network. The differential signal is obtained through a balun while a residual common-mode signal appears from the same balun. To determine Γ, either (3a) or (3b) is theoretically sufficient. For a perfect balun, the common-mode signal is eliminated and thus only (3a) will be applied to the computation. In practice, since imbalance in the balun is unavoidable, the common-mode noise cannot be completely eliminated. This common-mode signal adds to the power reading which in turn effects to the performance.

B. Calibration method

In order to measure Γ by using the proposed differential SPR structure, a calibration procedure is needed to determine the characteristic parameters of the differential SPR. The systematic errors caused by the non-ideal characteristics of the SPR hardware can also be removed in the calibration process. To calibrate the differential SPR, the power equation shown in (3a) is applied. By substituting k=3, 4, 5 and 6 in (3a) and perform mathematical manipulation, we obtain a calibration equation system presented in matrix form as follows:-

$$\begin{bmatrix} P_{d3} \\ P_{d4} \\ P_{d5} \\ P_{d6} \end{bmatrix} = |b_2|^2 \begin{bmatrix} C_{11} & C_{12} & C_{13} & C_{14} \\ C_{21} & C_{22} & C_{23} & C_{24} \\ C_{31} & C_{32} & C_{33} & C_{34} \\ C_{41} & C_{42} & C_{43} & C_{44} \end{bmatrix} \begin{bmatrix} 1 \\ |\Gamma|^2 \\ \mathrm{Re}\{\Gamma\} \\ \mathrm{Im}\{\Gamma\} \end{bmatrix} \quad (4)$$

where $\boldsymbol{C}$ is the characteristic matrix for the differential SPR. $P_{dk} = |b_{dk}|^2$ is the differential-mode power that is obtained through the balun at port k, where k=3, 4, 5, 6. In this case, $\boldsymbol{C}$ can be determined with several calibration schemes; for example five standard loads can be used for calibration [19]. Consequently, the real and imaginary parts of Γ can be solved from (4) by performing matrix inversion, resulting in the following equations:-

$$\mathrm{Re}\{\Gamma\} = \frac{\sum_{j=1}^{4} x_{3j} \cdot P_{d\,2+j}}{\sum_{j=1}^{4} x_{1j} \cdot P_{d\,2+j}} \quad (5a),$$

$$\mathrm{Im}\{\Gamma\} = \frac{\sum_{j=1}^{4} x_{4j} \cdot P_{d\,2+j}}{\sum_{j=1}^{4} x_{1j} \cdot P_{d\,2+j}} \quad (5b),$$

where x_{ij} denotes the element at row i and column j of $\boldsymbol{C}^{-1}$. $P_{d\,2+j}$ denotes the differential-mode power obtained through the balun; for j = 1-4, this leads to P_{d3}, P_{d4}, P_{d5} and P_{d6}, respectively. The solution for Γ in (5) is found in a similar manner to the technique proposed by Hoer [19] and several calibration algorithms [20]-[22] can also be applied for the differential SPR.

III. Analysis of Common-mode Rejection Ratio (CMRR)

In the differential SPR structure shown in Fig. 1, the differential-mode operation is obtained with differential transmission lines and baluns. In practice, common-mode noise and unbalanced effects can occur due to non-ideal behavior relating to the power source, grounding system, differential transmission lines and baluns used in the design. This will degrade the differential SPR performance. To quantify the performance of the proposed differential SPR,

common-mode rejection ratio (CMRR) analysis is applied. Normally, CMRR is defined by the differential-mode transmission versus the common-mode signal transmission from the input port (port A) to output port (port B) as follows [14];-

$$CMRR = 20\log_{10}\left|\frac{S_{ddBA}}{S_{ccBA}}\right| \quad (6),$$

where CMRR is in decibels (dB). S_{ddBA} and S_{ccBA} denote the differential transmission coefficients and common mode transmission coefficients from input port A to output port B, respectively. Similarly, the CMRRs of the 2-port differential transmission line that is used in the proposed differential SPR can be defined as follows,

$$CMRR_{21} = 20\log_{10}\left|\frac{S_{dd21}}{S_{cc21}}\right| \quad (7a),$$

$$CMRR_{12} = 20\log_{10}\left|\frac{S_{dd12}}{S_{cc12}}\right| \quad (7b),$$

where $CMRR_{21}$ and $CMRR_{12}$ refer to the CMRR from differential port 1 to 2 and port 2 to 1, respectively. S_{dd21} and S_{dd12} are differential-mode transmission parameters from port 1 to 2 and from port 2 to 1, respectively. S_{cc21} and S_{cc12} are common-mode transmission parameters from port 1 to 2 and from port 2 to 1, respectively.

For the 3-port balun circuit that is used in the proposed differential SPR, the CMRR is defined in a different way since the common-mode port is unavailable at the single-ended port of the balun. This can be defined as follows [14];-

$$CMRR_{ds} = 20\log_{10}\left|\frac{S_{ds}}{S_{cs}}\right| \quad (8a),$$

$$CMRR_{sd} = 20\log_{10}\left|\frac{S_{sd}}{S_{sc}}\right| \quad (8b),$$

where $CMRR_{ds}$ and $CMRR_{sd}$ refer to the single-ended to differential ports and from differential to single-ended ports, respectively. S_{ds} and S_{cs} denote the transmission coefficients from single-ended port to differential and to common modes, respectively. S_{sd} and S_{sc} are the transmission coefficients from differential and common-mode to single-ended modes, respectively.

By applying the CMRR definitions of differential line and balun circuit to the proposed differential SPR shown in Fig. 1, we define its CMRR as the ratio between the differential and common-mode signal transmissions at power reading port k (k being 3, 4, 5 or 6) referred to the single-ended RF input port 1 as follows,

$$CMRR_{k1} = 20\log_{10}\left|\frac{S_{dk1}a_1}{S_{ck1}a_1}\right| \quad (9)$$

Eliminating a_1, by using (3b) and rewriting in term of Γ, we obtain,

$$CMRR_{k1} = 20\log_{10}\left|\frac{(S_{dk2}S_{21}-S_{dk1}S_{22})\Gamma+S_{dk1}}{(S_{ck2}S_{21}-S_{ck1}S_{22})\Gamma+S_{ck1}}\right| \quad (10)$$

From (10), it is shown that the CMRR of the proposed differential SPR is a function of the load, with reflection coefficient Γ, at port 2. This means that to evaluate the CMRR of the differential SPR, various DUT measurements are required - in particular, five standard loads Γ of 0, -1, 1,+j and -j. However, S_{ck1} and S_{ck2} in (10) will not be obtained by direct measurement since the common-mode signal is unavailable at single-ended port of the 3-port balun. In this paper, S_{dki}, and S_{cki} where i is either 1 or 2, can be obtained by the steps given below:-

Step 1: Measure the 3-port single-ended S-parameters of the balun connected at power reading port k. Convert the single-ended S-parameters of the balun to mixed-mode S-parameters.

Step 2: Measure the 3-port single-ended S-parameter of the differential SPR structure. These three single-ended ports are port i, k^+ and k^-. Noted that port k^+ and k^- are differential ports of differential line at power reading port k that is connected to the balun, and can be measured by removing the balun at power reading port k.

Step 3: Convert the 3-port single-ended S-parameters obtained from *Step 2* to mixed-mode S-parameters.

Step 4: Connect the mixed-mode S-parameters obtained from *Step 1* and *Step 3* in the flow graph shown in Fig.3.

The above measurement procedure is based on a two-port network analyzer measurement. During the measurement procedure, only two ports are measured and the other ports are terminated by its characteristics impedance. This is similar to the 3-port balun S-parameter extraction [23].

In Fig. 3, the mixed-mode S-parameters obtained from *Step 3* are indicated with the bar symbol. The symbol i can be either 1 or 2, for port 1 or port 2 of the differential SPR and k={3, 4, 5, 6} for the power reading ports. The dark, gray and dotted lines represent the differential-mode, common-mode and conversion-mode paths, respectively. From Fig. 3, we apply Mason's rule [24] to solve for S_{dki} and S_{cki}, giving the expressions (11a) and (11b).

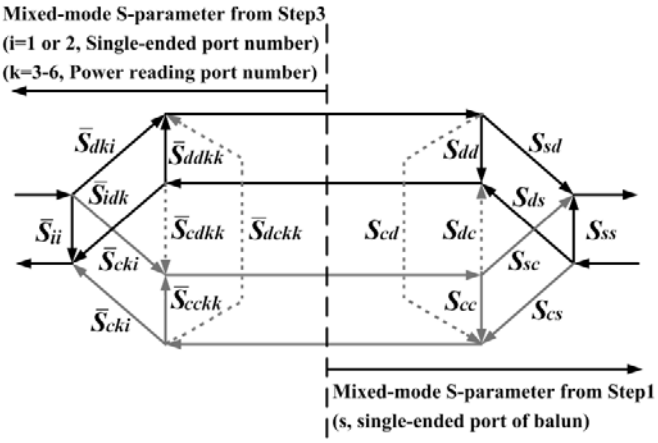

Fig. 3 Signal flow graph for calculating S_{dki} and S_{cki}

$$S_{dki} = \frac{(\bar{S}_{dki}S_{sd})\left(1-(\bar{S}_{dckk}S_{cd}+\bar{S}_{cckk}S_{cc})\right)+\bar{S}_{dki}S_{sc}(S_{dd}\bar{S}_{cdkk}+S_{cd}\bar{S}_{cckk})}{1-(\bar{S}_{ddkk}S_{dd}+\bar{S}_{cdkk}S_{dc}+\bar{S}_{cckk}S_{cc}+\bar{S}_{dckk}S_{cd})+\bar{S}_{ddkk}\bar{S}_{cckk}(S_{dd}S_{cc}-S_{dc}S_{cd})+\bar{S}_{dckk}\bar{S}_{cdkk}(S_{dc}S_{cd}-S_{dd}S_{cc})} \quad (11a)$$

$$S_{cki} = \frac{(\bar{S}_{cki}S_{sc})\left(1-(\bar{S}_{ddkk}S_{dd}+\bar{S}_{dckk}S_{cd})\right)+\bar{S}_{cki}S_{sd}(S_{dc}\bar{S}_{ddkk}+S_{cc}\bar{S}_{dckk})}{1-(\bar{S}_{ddkk}S_{dd}+\bar{S}_{cdkk}S_{dc}+\bar{S}_{cckk}S_{cc}+\bar{S}_{dckk}S_{cd})+\bar{S}_{ddkk}\bar{S}_{cckk}(S_{dd}S_{cc}-S_{dc}S_{cd})+\bar{S}_{dckk}\bar{S}_{cdkk}(S_{dc}S_{cd}-S_{dd}S_{cc})} \quad (11b)$$

TABLE I. DIMENSIONS OF SYMMETRICAL CPS ON FR4 SUBSTRATE
(substrate height=1.6 mm, copper thickness=0.05mm, ε_r=4.55, tan δ =0.02)

Characteristic impedance (Ω)	Width (mm)	Separation (mm)
50	3	0.14
100	2.54	0.48
200	2.54	4.30

IV. DIFFERENTIAL SAMPLED-LINE SPR

To demonstrate the differential SPR concept, a sampled-line SPR (SL-SPR) based on a purely differential transmission line without reference ground plane is considered, as illustrated in Fig. 4. This SL-SPR is proposed as a simple development of the single-ended structure [12]. The differential SPR uses a differential transmission line realized in the coplanar strip (CPS) medium [25]. The two ends of the CPS line are connected to the baluns at port 1 and port 2, respectively. The RF signals are sampled from ports 3 to 6 using coupling resistors, as previously reported for the single-ended, microstrip-based, SL-SPR [26]. The sampled RF power is subsequently converted to DC voltages by RF detector.

To validate the system operation, the CPS sampled-line six-port network is designed and simulated with Agilent ADS™ and Ansoft HFSS™ software, as described in subsection IV(A). The CMRR of the CPS sampled-line six-port network is then calculated based on the simulated results.

A. Symmetrical CPS design

The dimensions of the symmetrical CPS line were calculated for a FR-4 substrate using a recognized synthesis tool [27] and the parameters for 50, 100 and 200 Ω lines are given in Table I (The lower impedance of CPS line allows low insertion loss of differential and common-modes). Impedances of 50 and 100 Ω are difficult to implement practically, so the characteristic impedance of 200 Ω was used, with 2.54 mm width and 4.30 mm gap. Commercially-available 1:4 balun transformers could be employed to the CPS design and allow measurement with a standard 50 Ω network analyzer. A quarter-wavelength of the selected CPS design is 45 mm long at 1 GHz. The performance of a CPS line with 70 mm length was verified by simulating with Ansoft HFSS™. The differential and common-modes of the CPS line were extracted by terminating all four ports of the symmetrical CPS line with characteristic impedance 100 Ω to ground and measuring single-ended S-parameters. The resulting four-port single-ended S-parameters of the CPS line were converted to mixed-mode S-parameters, which are plotted in Fig. 5.

Fig. 5(a) shows the differential and common-mode transmission responses of the symmetrical CPS line. In Fig. 5(a)-5(b), it is clear that the designed CPS line can support differential-mode signals better than the common mode. Low cross-mode conversion is obtained as shown in Fig. 5(c). The computed CMRR of the CPS line is shown in Fig. 5(d). More than 3 dB CMRR at 1 GHz is obtained.

B. Differential sampled-lined six-port network

Next, the complete differential sampled-line six-port network, as shown in Fig. 4, was modeled. The CPS line is 70 mm long and each differential port is separated with a 10 mm gap. To couple the RF signal from the CPS line, a large resistor coupling is required to minimize the insertion loss performance of CPS line and keep the RF coupled signal within the working range of commercial RF detectors. A 2 kΩ lumped resistor is applied for coupling RF signals from the CPS line, with each single-ended power measurement port set to 100 Ω impedance. The 100 Ω is single-ended characteristic impedance of the 200 Ω differential line CPS and the differential port of balun. The differential sampled-line six-port network was simulated with Ansoft HFSS™. Twelve single-ended S-parameters are obtained. The mixed-mode S-parameters were calculated [28] and are plotted in Fig. 6.

Fig. 6(a) shows the differential and common-mode transmission coefficients from port 1 to 2. In Fig. 6(a), the differential transmission coefficient is better than -4 dB, while the differential reflection coefficient is less than -17 dB. Around 1 GHz, the common-mode transmission and reflection coefficients are less than -4 and -3 dB, respectively. The minimum common-mode transmission coefficient is -14 dB at 1.26 GHz. This means that the differential SL six-port network achieves low common-mode signal transmission between port 1 and 2. Fig. 6(b) and 6(c) show the differential and common-mode transmission coefficients from port 1(or 2) to the power reading port (port 3 to 6), respectively. Eight differential and eight common-mode transmission coefficients are plotted. Low differential signal transmission is obtained because a design with large coupling resistors is chosen. It should be noted that the differential transmission coefficient of the SL six-port network and its frequency characteristics depend on the coupling resistors.

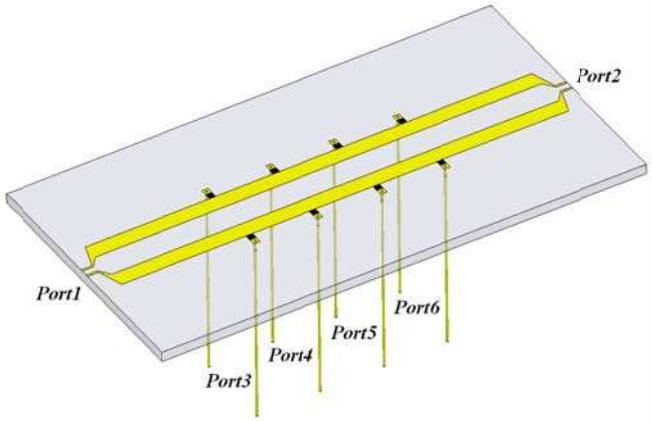

Fig. 4 Differential sampled-line six-port network for HFSS™ simulation

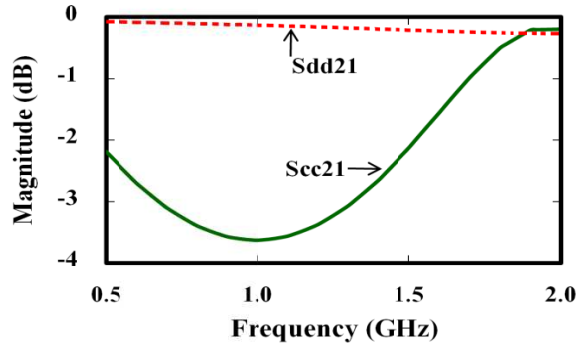

(a)

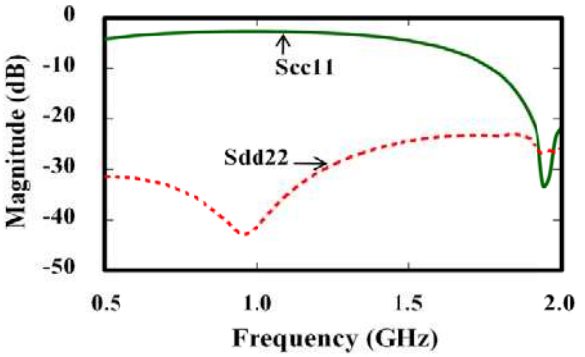

(b)

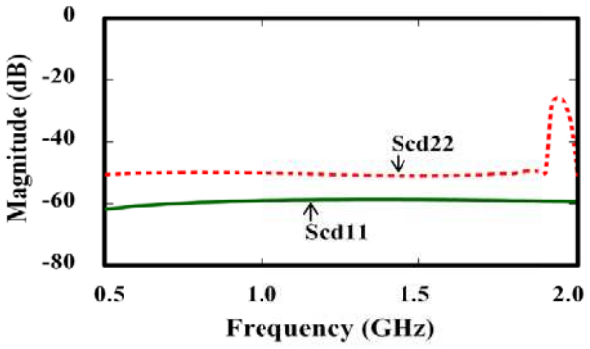

(c)

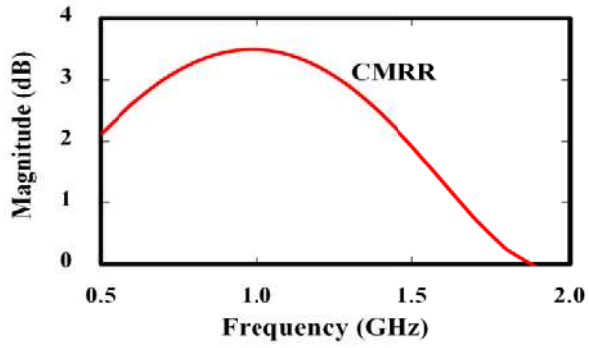

(d)

Fig. 5 Computed mixed-mode S-parameters of the CPS line, (a) Transmission for differential mode, (b) Reflection for differential mode, (c) Cross-mode conversion, and (d) Common-mode rejection ratio.

C. Differential SL six-port network with ideal baluns

Here, the differential SPR shown in Fig. 1 is modeled by combining the differential sampled-line six-port network simulation as described in Section IV(C) with six ideal 1:2 baluns. The performances of the SPR in terms of CMRRs,

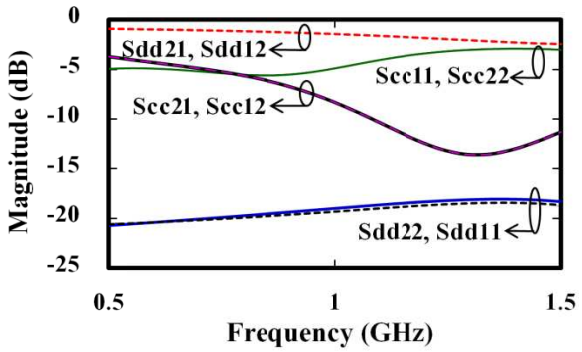

(a)

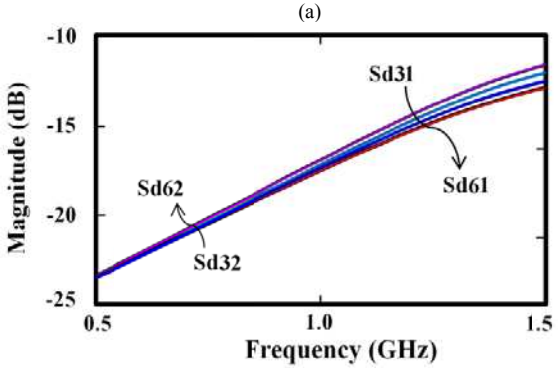

(b)

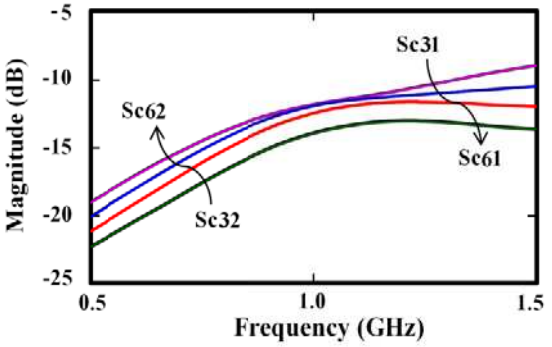

(c)

Fig. 6 Simulated mixed-mode S-parameters of the differential sampled-line six-port network: (a) Differential-mode and common-mode transmission coefficients from port 1 to 2, (b) Differential-mode transmission coefficients from port 1 and 2 to ports 3 to 6, and (c) Common-mode transmission coefficients from port 1 and 2 to ports 3 to 6

differential and common-mode transmission can be calculated from (10)-(11b). Figs. 7(a), (b) and 7(c) show the calculated single-ended, differential and common-mode S-parameters obtained from (12a) and (12b), respectively. In Fig. 7(a), the calculated differential-mode S-parameters are similar to that of the differential SL six-port network shown in Fig. 6(a). In Fig. 7(c), the common-mode transmission coefficients at the power sampling ports, either referred to port1 or 2, are very low. Such negligible common-mode transmissions are a result of using ideal baluns, which have an excellent capability to eliminate common-mode signals.

Figs. 7(e)-7(g) show the calculated CMRRs of ports 3 to 6 referred to port 1. The differential SL six-port network designed with ideal baluns is terminated with five different loads. The results are obtained by applying the S-parameters shown in Fig. 7(a)-7(c) to eqns. (10)-(11b). As shown, the CMRRs vary with the terminating load at port 2. The obtained

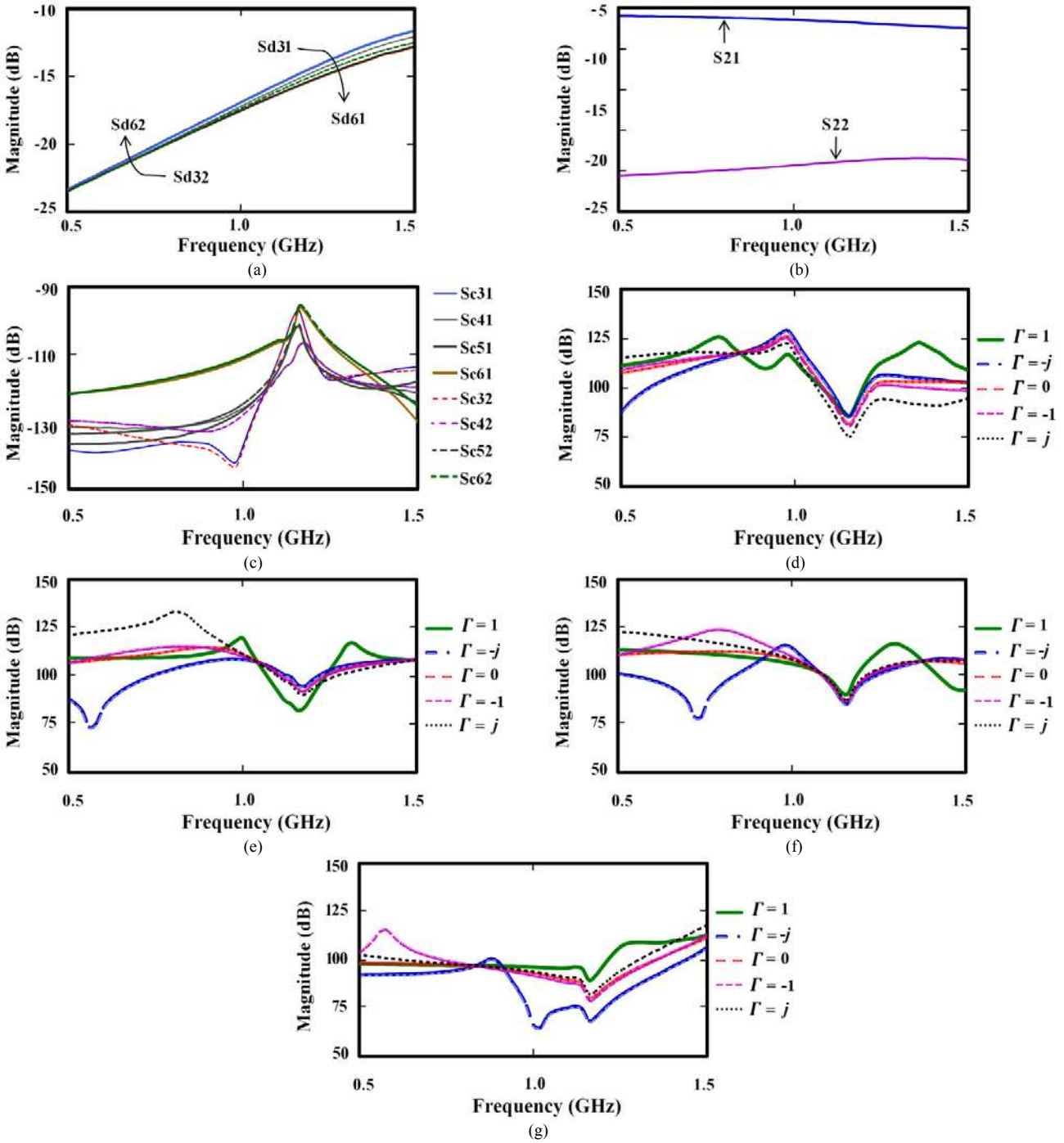

Fig. 7 Simulated performance of the differential sampled-line six-port network with ideal baluns: (a) Differential mode transmission, (b) Single-ended mode transmission, (c) Common-mode transmission, (d) CMRR at port 3, (e) CMRR at port 4, (f) CMRR at port 5, and (g) CMRR at port 6.

CMRRs at all power sampling ports are better than 60 dB, which is mainly due to the ideal balun performance. Clearly the actual balun performance is very important for eliminating common-mode noise in the proposed differential SPR – more so than the CPS differential line performance. This is because the CMRR of the balun is much greater than the CPS differential line.

D. Performance for impedance measurement

In this section, the proposed differential SPR is simulated to predict its behavior with several load impedances. The simulation is performed for two different design cases – with ideal and imperfect baluns. In practice, baluns will always exhibit imbalance and we model this by inserting a phase shifter and attenuator to artificially produce imbalance effects as illustrated in Fig. 8. The phase shifter and attenuator are varied from ±20 degree and ±2 dB, respectively, to producing imbalance effects. For the ideal balun case, the phase shifter and attenuator are set to zero.

Prior to impedance measurement, a calibration process is performed at frequencies around 1 GHz. The 1 GHz simulated

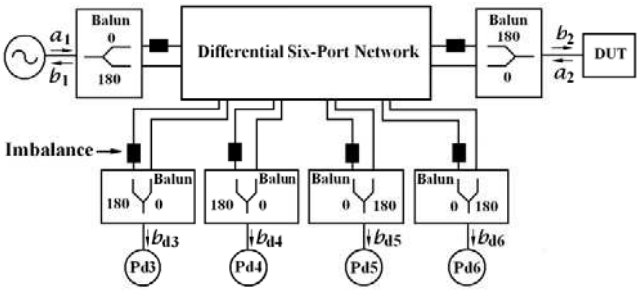

Fig. 8 Simulation setup to test imbalance effect for differential SPR

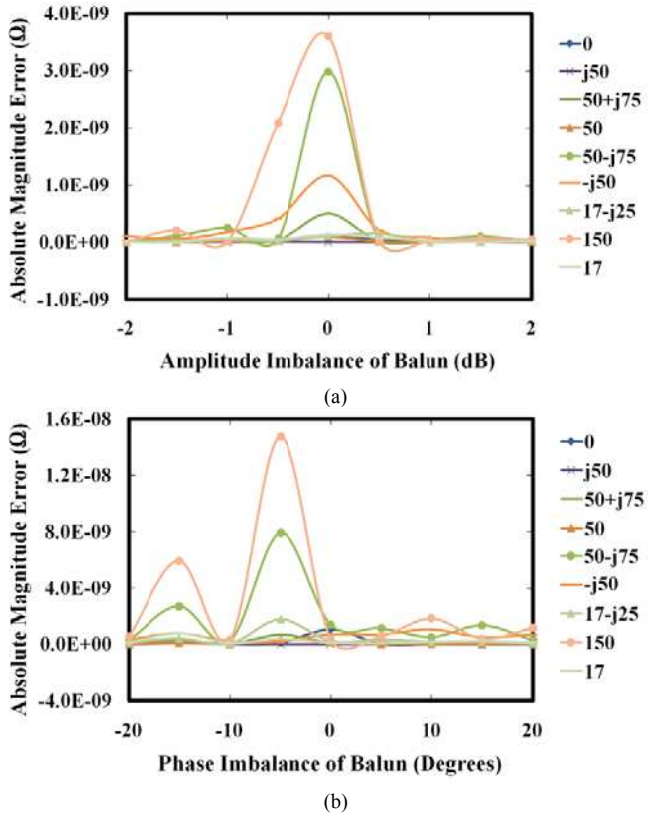

Fig. 9 Simulation results of imbalance effect for differential SPR: (a) Amplitude imbalance and (b) Phase imbalance

results of the SPR with amplitude imbalance and phase imbalance of baluns are illustrated in Fig. 9(a) and (b), respectively. The magnitudes of the error between the calculated and the actual load impedances are computed to quantify the impedance measurement performance of the differential SPR. As shown, we obtain very accurate results. We performed the impedance measurement at other frequencies and still obtained accurate results. This suggests that imbalance effect in the baluns can be removed by the calibration process.

V. Design and Measurement

The differential SPR structure was designed and fabricated on FR4 substrate for operation at 1 GHz. A symmetrical CPS line with 2.54 mm width and 4.30 mm separation was selected to achieve 200 Ω differential characteristic impedance. Murata 50-to-200 Ω baluns [29] were selected (part no. LDB21942M20C-001) as the differential port is matched to

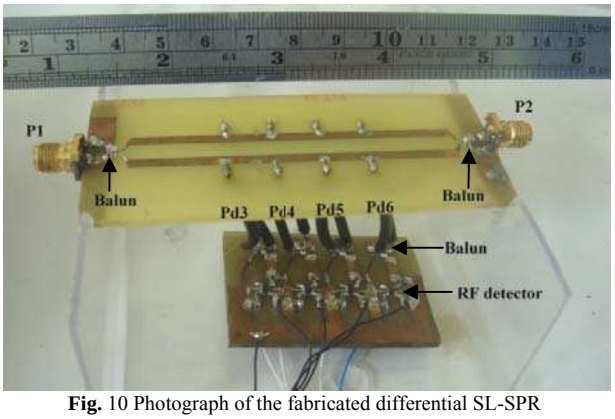

Fig. 10 Photograph of the fabricated differential SL-SPR

the 200 Ω characteristic impedance of differential line CPS and the single-ended port can be measured by a standard 50 Ω network analyzer. The RF differential signals are coupled from the CPS line by using 2 kΩ lumped SMT resistors (style 0603). The RF signal coupling obtained with 2 kΩ coupling resistors is about -17 dB, which suits the dynamic range of the chosen power detector. LT®5534 logarithmic power detectors [30] are used for determining the RF differential power from the baluns. Its input impedance (50 Ω) is matched to the single-ended port of the balun, and it has wide dynamic range (0 to -60 dBm) that can cover the range of power readings from the differential CPS line. On-board 12-bit analog to digital converters are connected to the detectors [31] to convert the DC signals from the detectors to binary data. The data is then transferred to a PC and the calculations performed using a program developed in LabVIEW™.

Fig. 10 shows a photograph of the fabricated differential SPR. Port 'P1' is connected to the RF source, port 'P2' is connected to the DUT and ports 'P3' to 'P6' are connected through baluns to the power-sampling detectors. Validation of the performance of the fabricated differential SPR is investigated and discussed in the following subsections. The performance of the baluns and the differential SL-SPR (CMRR and impedance measurement accuracy) are considered in detail.

A. Balun

As mentioned previously, the balun is the key component in the design for reducing unwanted common-mode noise. Thus, knowledge of the S-parameters of the balun is needed to evaluate the performance of the proposed differential SPR. Unfortunately, the 3-port S-parameters of the LDB21942M20C-001 Murata balun were unavailable. So, the S-parameters of the balun were obtained by measuring a set of 2-port single-ended S-parameters with the third port connected to a matched load. This process is repeated to all balun ports so that all the elements in the 3-port S-parameter of the balun are obtained.

After the 3-port S-parameters were obtained, the mixed-mode S-parameters of the balun were calculated. Fig. 11 shows the computed mixed-mode S-parameters, derived from the measured single-ended S-parameters of the LDB21942M20C-001 balun. Fig. 11(a) shows the reflection and cross-mode transmission coefficients of the balun. It can be seen that the differential reflection coefficient is well below

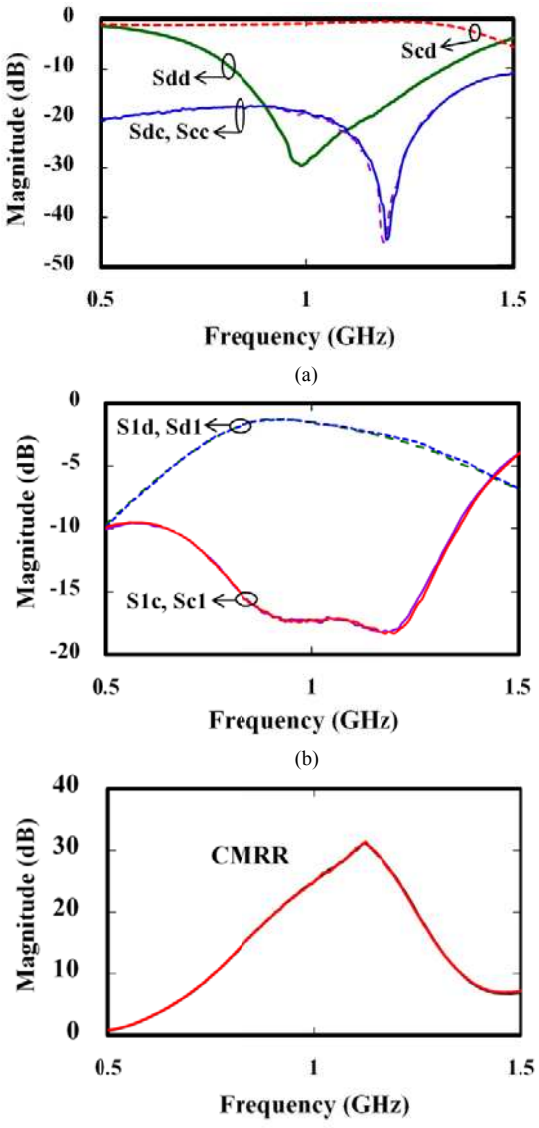

Fig.11 Measured S-parameters of the balun (a) Reflection and cross-mode transmission coefficients, (b) Transmission coefficient, and (c) Common-mode rejection ratio.

-25 dB, the cross-mode transmission coefficient between differential and common-mode is less than -15 dB while the common-mode reflection coefficient is better than -5 dB at 1 GHz, respectively. Fig. 11 (b) shows the transmission coefficients and it can be seen at 1 GHz that the differential transmission coefficient is better than -3 dB while the common-mode transmission coefficient is well below -17 dB. This confirms that the performance of the balun is sufficient for both differential and common-mode ports at the operating frequency. As shown in Fig. 11(c), the computed CMRR is better than 20 dB at 1 GHz, meaning that the balun can be used to reduce the common-mode noise effectively.

B. CMRR of the differential SL-SPR

To evaluate the CMRR of the fabricated differential SL-SPR, the measured single-ended S-parameters of the differential SL six-port network and baluns are required. The simulated S-parameters of the differential six-port network obtained from Ansoft HFSS™ are compared with the measured results. The S-parameters of the fabricated differential SL-SPR were measured by using 2-port single-ended measurements made with the other ports terminated with matched loads. A comparison of these results is illustrated in Fig. 12.

Fig. 12(a) shows the transmission and reflection coefficients between port 1 and 2. It can be seen that the transmission coefficient is better than -6 dB while the reflection coefficient is less than -15 dB. Good agreement between simulated and measured results is obtained. Figs. 12(b)-12(e) show the transmission coefficients from port 1 or 2 to the power sampling ports (ports 3 to 6). Values well below -15 dB are achieved over the range 0.8-1.25 GHz.

Fig. 13 shows the calculated CMRRs at the power sampling ports of the differential SL-SPR for five DUT reflection coefficients. Comparing with the CMRRs of the balun itself, shown in Fig. 11 (c), it can be confirmed that the CMRR response of the differential SL-SPR is mainly governed by the balun performance. Thus, a careful selection for the balun is a key to achieving a high-performance differential SPR that has good capability to suppress common-mode noise and interference.

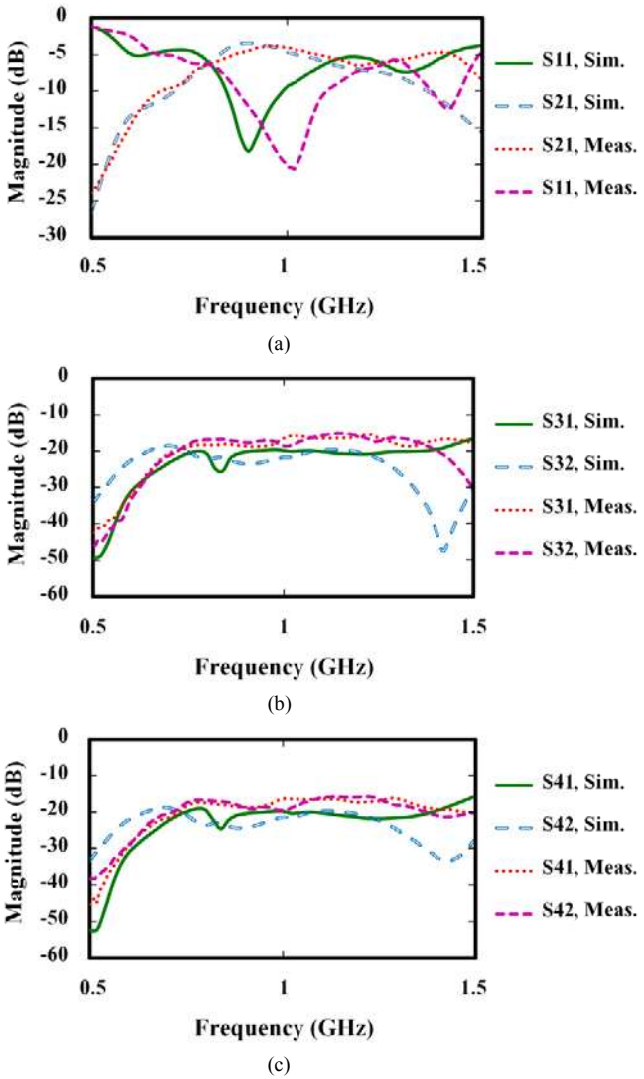

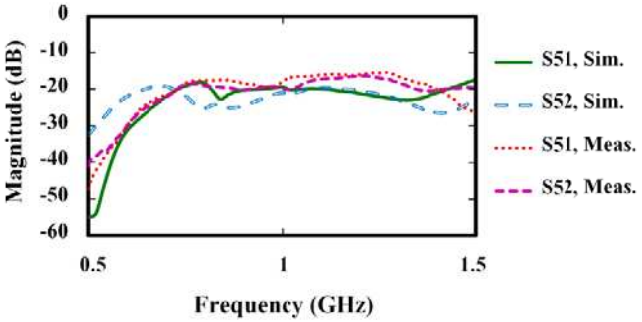

(d)

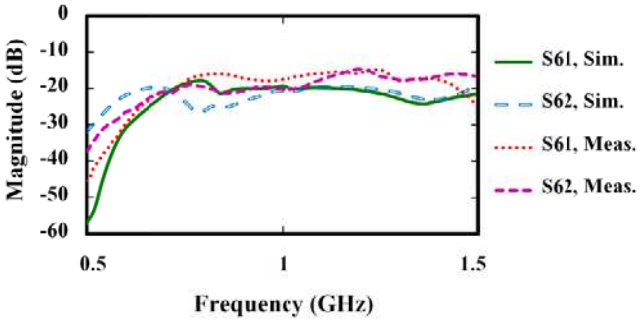

(e)

Fig. 12 Measured results of the fabricated differential SL-SPR, (a) Transmission and reflection coefficients of ports 1 and 2, (b) Transmission coefficients of ports 1 and 2 to port 3, (c) Transmission coefficients of ports 1 and 2 to port 4, (d) Transmission coefficients of ports 1 and 2 to port 5 and (e) Transmission coefficients of ports 1 and 2 to port 6.

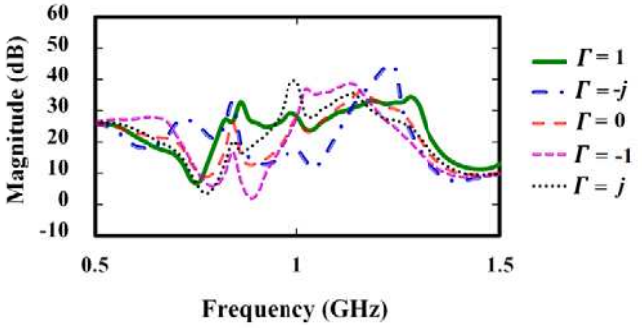

(a)

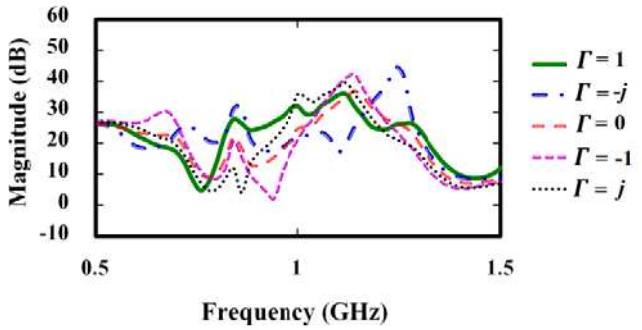

(b)

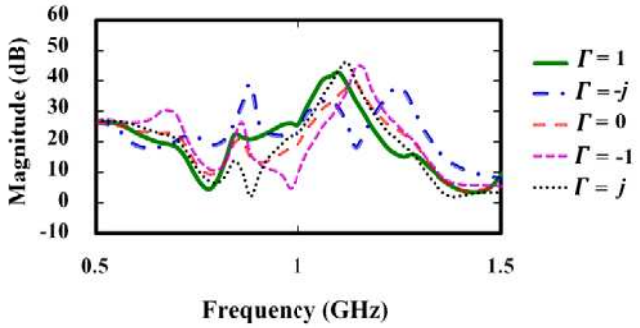

(c)

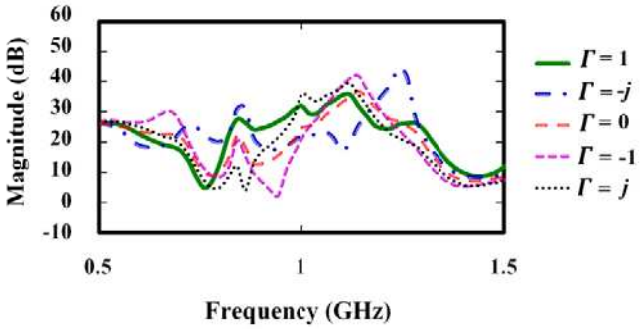

(d)

Fig. 13 Calculated CMRRs at port, (a) 3, (b) 4, (c) 5 and (d) 6

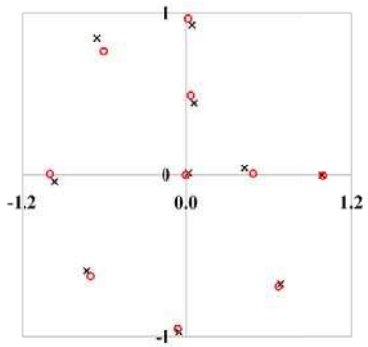

(a)

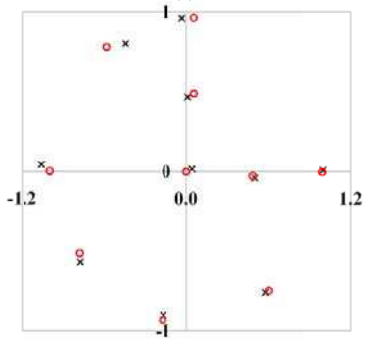

(b)

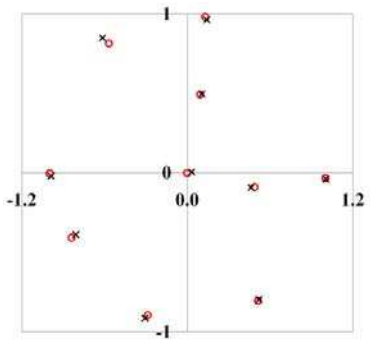

(c)

Fig.14 Measured reflection coefficients of the differential SPR structure (**x**), compares to automatic network analyzer (**o**) at (a) 0.950 GHz, (b) 0.975 GHz and (c) 1 GHz

C. Reflection coefficient measurement

The reflection coefficient measurement of the proposed differential SPR structure is demonstrated and discussed in this subsection at frequencies around 1 GHz. Prior to reflection coefficient measurement, calibration must be performed to eliminate the systematic noise and some uncertainties in the measurement system from various components such as the logarithmic detector and analog-to-digital converter. To counteract these uncertainties, a calibration scheme based on a statistical method that uses the weighted squared error technique [22] was chosen. This was achieved by applying (7a) and (7b). After calibration was performed, measurements on ten different DUTs were carried out. These measurements are compared to those obtained from a commercial automatic vector network analyzer (HP8510C) in Fig. 14. Figs. 14(a)-14(c) show the reflection coefficient measurements made with the differential SPR at three frequencies - 0.95 GHz, 0.975 GHz and 1 GHz. It is found that the measured results of the proposed differential SPR are close to the measured results from the 8510C network analyzer. The mean absolute errors compared to the results obtained from the network analyzer are 0.032, 0.029 and 0.033 at 0.95 GHz, 0.975 GHz and 1 GHz, respectively.

D. Interference rejection in the differential SPR

In this subsection, the performance of the differential SPR in a hostile electromagnetic environment is investigated and compared to the single-ended SPR. A 2.5 GHz rectangular microstrip patch antenna on Duroid 5880 substrate (substrate height=0.787 mm, copper thickness=0.017 mm, ε_r=2.20, tan δ =0.0009) is chosen to generate the electromagnetic wave interference with the differential and single-ended SPRs, as illustrated in Fig. 15. This antenna has patch size 12x16 mm and a feed line 2x10 mm that is connected to the wide side at distance 2 mm away from the edge of the patch). The patch antenna is placed above the center of the differential and single-ended SPRs at a distance of 150 mm. The input signal to the patch antenna was varied from -20 to +5 dBm. This emulates common-mode noise in the SPR systems. To validate the common-mode rejection of the differential SPR, the reflection coefficient of various electrical loads that cover the Smith Chart area were measured by the differential and single-ended SPR with and without the 2.5 GHz inference present, respectively.

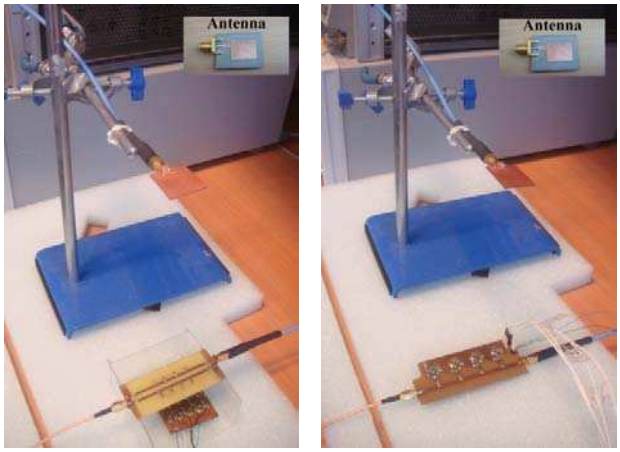

(a) (b)

Fig. 15 Experimental setup to investigate the effect of electromagnetic wave interference on: (a) differential SPR and (b) single-ended SPR

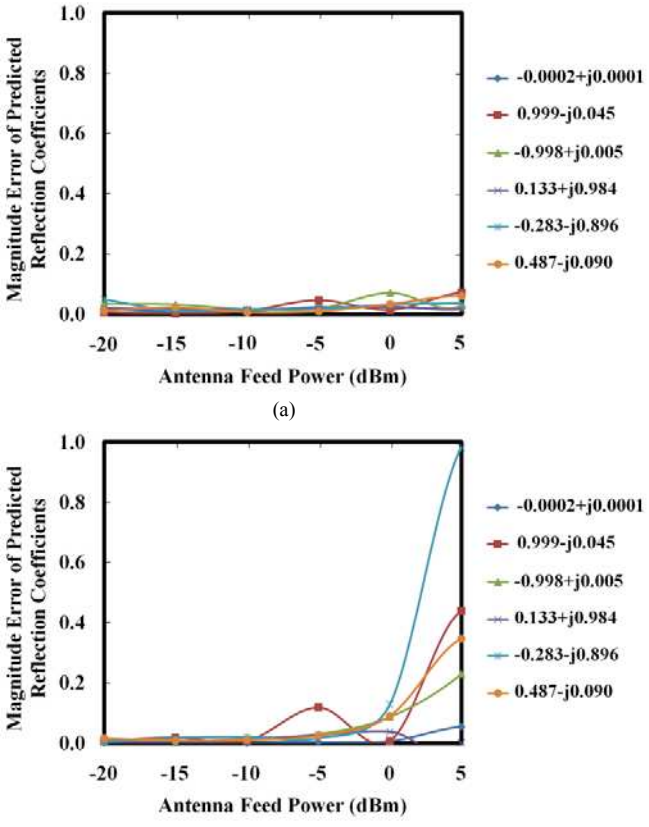

(a)

(b)

Fig.16 Effect of emulated interference on (a) differential SPR and (b) single-ended SPR measurements.

Fig. 16 (a) and (b) show the magnitude error of reflection coefficients at 1 GHz when using the differential and single-ended SPRs, respectively, in the presence of interference. From -20 to -10 dBm interference signal power, the reflection coefficient error for the single-ended SPR is comparable to the differential SPR. However, as the antenna feed power is increased beyond -10dBm, it can be seen that the single-ended SPR is no longer useable at all, whilst the differential SPR still maintains its performance thanks to its common-mode rejection. It should be noted for completeness that the

reflection coefficient error of different electrical loads is not equal as the common-mode rejection ratio is a function of load reflection coefficient.

VI. Conclusions

The analysis and design of a differential six-port reflectometer has been presented. The system has been demonstrated experimentally at 1 GHz and produced DUT measurements that match the results from a commercial vector network analyzer. The proposed differential SPR structure aims to reduce the inherent common-mode noise in the system. The differential SPR structure is composed of a sampled-line differential six-port network with baluns. The balanced ports of the baluns are connected to the differential six-port network while the single-ended ports serve as the interface with the signal source, DUT and RF detectors. Determination of the DUT reflection coefficient with the differential SPR structure has been analyzed by using mixed-mode S-parameters as well as studying the common-mode rejection ratio. The effect of imbalance of the balun can be removed by the calibration procedure prior to the measurement. From the CMRR results, it is shown that the technique is capable of reducing the common-mode noise. It is noted that the common-mode noise rejection ratio depends mainly on the performance of balun rather than CPS differential line, which is clearly one of the key components determining the rejection of common-mode noise and interference. The reflection coefficient measurements obtained from the proposed differential SPR are in good agreement with the commercial network analyzer. It is believed that the proposed differential SPR structure will find various applications for reflection coefficient measurement where common-mode noise or interference is of concern.

Acknowledgment

This research is supported by The Thailand Research Fund (TRF) for The Royal Golden Jubilee (RGJ) Ph.D Program Scholarship (PHD/0193/2551) and Prince of Songkla University.

References

[1] G. F. Engen, "The six-port reflectometer: An alternative network analyzer," *IEEE Transactions on Microwave Theory and Techniques*, vol. 25, no. 12, pp. 1075- 1080, Dec. 1977.

[2] G. F. Engen, "An improved circuit for implementing the six-sort technique of microwave measurements," *IEEE Transactions on Microwave Theory and Techniques*, vol. 25, no. 12, pp. 1080- 1083, Dec. 1977.

[3] C. A. Hoer, "A network analyzer incorporating two six-port reflectometers," *IEEE Transactions on Microwave Theory and Techniques*, vol. 25, no. 12, pp. 1070- 1074, Dec. 1977.

[4] F. M. Ghannouchi and R. G. Bosisio, "Measurement of microwave permittivity using a six-portreflectometer with an open-ended coaxial line," *IEEE Transactions on Instrumentation and Measurement*, vol. 38, no. 2, pp. 505-508, Apr. 1989.

[5] J. Munoz, M. Rojo, and J. Margineda, "A method for measuring the permittivity without ambiguity using six-port reflectometer," *IEEE Transactions on Instrumentation and Measurement*, vol. 42, no. 2, pp. 222-226, Apr. 1993.

[6] J. A. R. Ball, B. Horsfield, J. R. Holdem, R. B. Keam, W. S. Holmes, and A. Green, "Cheese curd moisture measurement using a six port reflectometer," presented at the Proc. Asia Pacific Microwave Conf., New Delhi, India, vol. 2, pp. 479–482.

[7] K. Y. Lee, "Development of a microwave instrumentation system for the determination of moisture content in oil palm fruits," 2008. [Online]. Available: http://psasir.upm.edu.my/5092/. [Accessed: 06-Oct-2011].

[8] S. Julrat, M. Chongcheawchamnan, T. Kaoraopaphong, O. Pattrapiboonchai, M. Krairiksh and I. D. Robertson, "Single frequency based dry rubber content determination technique for in-field measurement application", *IEEE Sensors Journal*, vol. 12(10), pp. 3019 – 3030, Oct. 2012.

[9] N. Seman and M. E. Bialkowski, "Design of a UWB 6-port reflectometer formed by microstrip-slot couplers for use in a microwave breast cancer detection system," in *2007 IEEE Antennas and Propagation Society International Symposium*, 2007, pp. 245-248.

[10] H. C. Lu and T. H. Chu, "Microwave diversity imaging using six-port reflectometer," *IEEE Transactions on Microwave Theory and Techniques*, vol. 47, no. 1, pp. 84-87, Jan. 1999.

[11] C. G. Miguelez, B. Huyart, E. Bergeault, and L. P. Jallet, "A new automobile radar based on the six-port phase/frequencydiscriminator," *IEEE Transactions on Vehicular Technology*, vol. 49, no. 4, pp. 1416-1423, Jul. 2000.

[12] A. Khy and B. Huyart, "A 94 GHz radar using a six-port reflectometer as a phase/frequency discriminator," in *Radar Conference, 2005. EURAD 2005. European*, 2005, pp. 213-215.

[13] B. Boukari, E. Moldovan, S. Affes, K. Wu, R. G. Bosisio, and S. O. Tatu, "A heterodyne six-port FMCW radar sensor architecture based on beat signal phase slope techniques," *Progress In Electromagnetics Research*, vol. 93, pp. 307-322, 2009.

[14] W. R. Eisenstadt, B. Stengel, and B. M. Thompson, *Microwave differential circuit design using mixed mode S-parameters*. Artech House Publishers, 2006.

[15] N. Yang, C. Caloz and K. Wu, "Greater than the sum of its part," *Microwave Magazine, IEEE*, vol 11, no. 4, pp. 69-82 June 2010.

[16] E. J. Griffin, "Six-port reflectometer circuit comprising three directional couplers," *Electronics Letters*, vol. 18, no. 12, pp. 491-493, Jun. 1982.

[17] K. Kurokawa, "Power waves and the scattering matrix," *IEEE Transactions on Microwave Theory and Techniques*, vol. 13, no. 2, pp. 194- 202, Mar. 1965.

[18] D. E. Bockelman and W. R. Eisenstadt, "Combined differential and common-mode scattering parameters: theoryand simulation," *IEEE Transactions on Microwave Theory and Techniques*, vol. 43, no. 7, pp. 1530-1539, Jul. 1995.

[19] C. A. Hoer, "Using six-port and eight-port junctions to measure active and passive circuit parameters," *NBS Tech, Note 673*, Sep. 1975.

[20] F. M. Ghannouchi and R. G. Bosisio, "An alternative explicit six-port matrix calibration formalism usingfive standards," *IEEE Transactions on Microwave Theory and Techniques*, vol. 36, no. 3, pp. 494-498, Mar. 1988.

[21] P. I. Somlo and J. D. Hunter, "A six-port reflectometer and its complete characterization by convenient calibration procedures," *IEEE Transactions on Microwave Theory and Techniques*, vol. 30, no. 2, pp. 186-192, Feb. 1982.

[22] S. P. Jachim and W. D. Gutscher, "A statistical method for calibrating the six-port reflectometerusing nonideal standards," *IEEE Transactions on Microwave Theory and Techniques*, vol. 37, no. 11, pp. 1825-1828, Nov. 1989.

[23] K. Jung *et al.*,"Marchand balun embedded probe," *IEEE Transaction on Microwave Theory and Techniques, IEEE Transactions*, vol.56, no.5, pp.1207-1214, May 2008

[24] N. S. Nise, *Control Systems Engineering*, 5th ed. Wiley, 2007.

[25] R. N. Simons, *Coplanar waveguide circuits, components, and systems*, John Wiley & Sons, Inc, 2001.

[26] B. M. Altrabsheh and I. D. Robertson, "A multi-probe microwave reflectometer using an improved calibration algorithm," in *Microwave Conference, 2006. 36th European*, 2006, pp. 979-982.

[27] J.W.P.Ng, "Ascps software version 1.1," 1999.

[28] L. B. Lok, "Balanced microwave circuit and adaptive single-sideband mixers", Ph.D. Thesis, University of Leeds, Leeds, London. May 2007.

[29] Murata Manufacturing Co., "Datasheet chip multilayer hybrid baluns LDB21942M20C-001".

[30] Linear technology cooperation, "Data sheet LT5534 50MHz to 3GHz RF power detector with 60 dB dynamic range", 2004.

[31] ARM Ltd., "Cortex-M3 technical reference manual", 2005.

Sakol Julrat obtained Bachelors degree in Mechatronics Engineering in 2005 and Master degree in Electrical Engineering in 2009 from Prince of Songkla University. He worked in hard disk drives industry for two years following the Bachelors degree. He is currently a Ph.D. student in Computer Engineering, Prince of Songkla University. His research interests are six-port application, dielectric measurement, sensors and measurement systems.

Mitchai Chongcheawchamnan was born in Bangkok, Thailand. He received the B.Eng.degree in telecommunication from King Mongkut's Institute of Technology Ladkrabang, Bangkok, in 1992, the M.Sc. degree in communication and signal processing from Imperial College, London, U.K., in 1995, and the Ph.D. degree in electrical engineering from the University of Surrey, Guildford, U.K., in 2001.
He joined the Mahanakorn University of Technology, Bangkok, in 1992, as a Lecturer. In 2008, he joined the Faculty of Engineering, Prince of Songkla University, Songkhla, Thailand, as an Associate Professor. His current research interests include microwave circuit design and microwave techniques for agricultural applications. Dr. Chongcheawchamnan is a member of the IEEE Microwave Society.

Ian Robertson holds the University of Leeds Centenary Chair in Microwave and Millimetre-Wave Circuits and is Head of the School of Electronic & Electrical Engineering. He has published over 400 papers in the area of microwave and millimetre-wave engineering as well as co-editing the well-known book RFIC and MMIC Design and Technology. He was elected Fellow of the IEEE in 2012 for contributions to MMIC design and millimetre-wave system-in-package technology. He was General Technical Programme Committee Chair for the 2011 European Microwave Week – the premier European event in microwave and millimetre-wave engineering. He has held over £3M in grants as PI and led 5 major EPSRC-funded collaborative projects. He currently leads an IeMRC-funded project in 3D microwave and millimetre-wave LTCC components with Loughborough and Imperial College. Prior to joining Leeds he was a founder member of the Advanced Technology Institute at the University of Surrey and led the MMIC Research Team at King's College London.